Nano Convergence
a SpringerOpen Journal

RESEARCH Open Access

A silicon nanowire photodetector using Au plasmonic nanoantennas

Sang-Won Jee[1,3], Keya Zhou[1,4], Dong-Wook Kim[2*] and Jung-Ho Lee[1*]

Abstract

We suggest a silicon nanowire (SiNW) photodetector side-contacted with hemispherical Au nanoantennas (NAs) that can remarkably amplify the intensity of the near-infrared optical field. The plasmonic NA suppresses visible-range guided mode excitation in SiNW, which enables our photodetector to possess a near-infrared-selective response and overcome the inherent poor optical absorption of Si. The NA can form Schottky contacts with SiNWs for enhancing carrier collection. The vertical NW array also has the geometrically beneficial effects of wide tolerance in light polarization with reduced material consumption.

Keywords: Si nanowire; Photodetector; Plasmonics; Subwavelength structure; Optical absorption; Plasmonic nanoantennas

1 Background

Si near-infrared (NIR) photodetectors are compatible with complementary metal oxide semiconductor (CMOS) technology [1], which can be fabricated with a production cost even lower than that of devices using other materials such as Ge [2] or InGaAs [3]. The indirect bandgap of Si (~1.12 eV), however, leads to poor optical absorption in the NIR region (750 nm < λ < 1100 nm), which hinders the development of Si photodetectors for optoelectronic on-chip integration. Semiconducting nanowires (NWs) might enable us to overcome the limitations of conventional bulk and thin film devices because of their unique geometrical advantages. NWs are known to possess an vastly larger optical cross-section than geometrical cross-section, due to the guided mode [4] and Fabry-Pérot resonances [5,6], as well as anti-reflection effects [7,8]. As a vertical platform of an NW array, spectral dependence of the optical response can be further modified via controlling its period, filling ratio, and symmetric arrangement [9-11]. Moreover, the radial *p-n* junctions offer an efficient carrier collection with the aid of orthogonal collection of charge carriers and incident photons [11-13]. Thus, there have been intensive studies to realize low cost and high efficiency NW-based optoelectronic devices [4-16].

Surface plasmon (SP) provides a new means to amplify the intensity of a local electromagnetic (EM) field, while tuning the optical responses throughout the visible-to-NIR spectral range [14-21]. It is known that the resonance energy of localized surface plasmon (LSP) is highly dependent on the geometry and dielectric functions of the metal nanoparticles (NPs) and supporting materials [17-19]. Thus, metallic NPs have been used as light harvesting nanoantennas (NAs), allowing efficient conversion of propagating light into a nanoscale confined, strong optical field [20-22]. Especially, Au NA shows a high radiation efficiency at long wavelengths (λ ≥ 600 nm) due to a large negative real part of dielectric function ε(ω), while Ohmic absorption losses are kept low with a small imaginary value of ε(ω) [20]. This guides us to simultaneously utilize the Si NWs and Au NA for the development of a new type of photodetector with enhanced NIR responsivity. Recently, there has been increasing research interest in optical and electrical characterizations of Si-based photodetectors with metallic NP [14-16]. Interesting works focused on either single NW devices [15,16] or sophisticated top-down fabrication [22] can offer useful insights to understand the fundamental mechanism; however, cost-efficient and simple fabrication methods are highly desirable for practical applications.

* Correspondence: dwkim@ewha.ac.kr; jungho@hanyang.ac.kr
[2]Department of Physics, Ewha Womans University, Seoul 120-750, South Korea
[1]Department of Chemical Engineering, Hanyang University, Ansan 426-791, South Korea
Full list of author information is available at the end of the article

Here, we propose SiNW-array-based plasmonic photodetectors with Au hemispherical NPs (hNPs) as optical NA, of which photoresponsivity in the NIR range is remarkably enhanced due to intriguing SP resonance effects at the hNP/Si interface. Excitation of the guided mode resonance in the SiNW is suppressed, since incoming light is dissipated and scattered by the hNPs at wavelengths (≤600 nm). The Au hNPs also form Schottky contacts with Si to promote efficient collection of photo-excited carriers. This approach provides an opportunity for low-cost fabrication of a highly sensitive SiNW NIR photodetector.

2 Methods

Vertical SiNW arrays (5 Ω-cm, 6 μm long) were fabricated on 15-μm-thick Si(n/n^+)-on-Insulator (SOI) wafers by metal-assisted electroless etching, in which the space filling ratio (FR) of SiNWs was ~0.28. Prior to the SiNW preparation, 50-nm-thick Au films were thermally evaporated on the wafers using a shadow mask to form top electrodes of the photodetectors. Subsequently, Ag nanoparticles were uniformly dispersed on the Si top surface while dipping in a mixed solution of de-ionized water, HF (4.8 M), and $AgNO_3$ (0.01 M) at 20°C for 1 min. Chemical etching was followed in a mixed solution of deionized water, HF (4.8 M), and H_2O_2 (0.5 M) to form a vertically aligned SiNW array with a diameter of 60 ± 33 nm. After etching, Ag nanoparticles that remained at the bottom of SiNWs were removed by nitric acid solution. Au was thermally evaporated onto the SiNWs with a very low deposition rate (0.1 Å/sec) so that the deposited Au agglomerated to form hNPs. Most hNPs were found within 1 μm from the top-ends of the SiNWs due to a directional tendency of thermal evaporation. Figure 1(a) and (b) show the scanning electron microscopy (SEM) and transmission electron microscopy (TEM) images of bare SiNW (BS) and Au NP-coated SiNW (AS) arrays, respectively. The histogram shows that the average diameter of AS is 20 ± 11 nm as shown in Figure 1(c). For Ohmic contacts, the backsides of SOI wafers were patterned using standard photolithography and etching of the oxide layer. The exposed backside n^+ regions of the wafers were attached to Au pads using Ag paste. Spectral photoresponses were measured using monochromatic light generated by a 300 W Xenon lamp. Photovoltaic measurements were carried out at one – sun illumination (AM 1.5G, 100 mW cm^{-2}) using a solar simulator (Peccel PEC-L11). The structural characterization of the NWs was carried out using field emission SEM (Hitach s-4800) and TEM (FEI Tecnai F30 Super-Twin). Nanoscale analyses using monochromated electron energy loss spectra (EELS) were carried out to estimate the SP energies for the Au NPs coated on SiNW. SiNWs suspended in isopropanol were dropped onto a carbon-coated copper grid for TEM and EELS observation.

3 Results and discussion

3-1 Optical Characteristics

To characterize the optical absorption properties of BS and AS arrays, a polydimethylsiloxane (PDMS) solution was allowed to infiltrate the wafer, and viscous PDMS

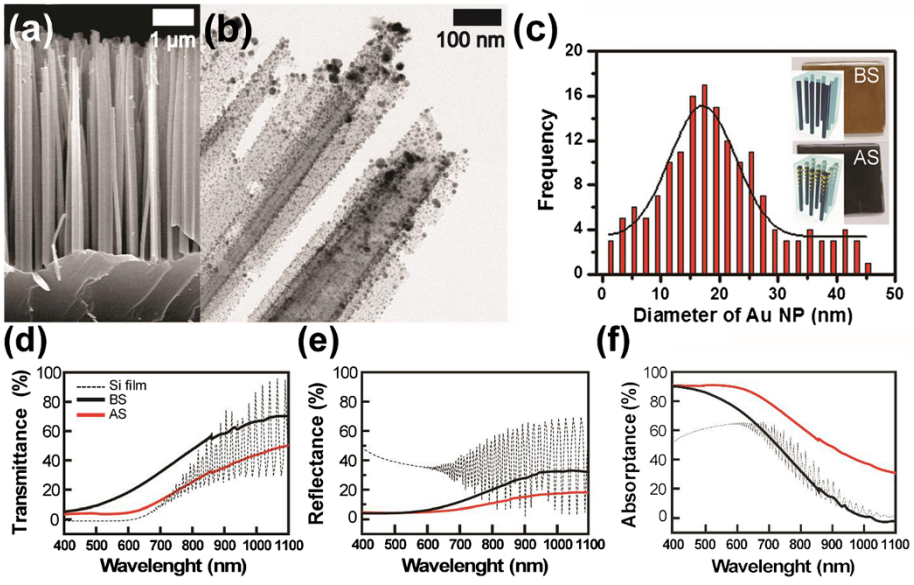

Figure 1 Morphology and optical features of bare SiNWs. (a) SEM image of bare SiNWs (BS, 6 μm-long) on a Si substrate. **(b)** TEM image of a top-end region (<1 μm) of Au NP-coated SiNWs (AS). **(c)** Histogram of the Au NP diameters in the AS arrays. (Insets show the illustration and optical photographs of BS and AS embedded in PDMS). The experimental optical spectra of BS (black) and AS (red) embedded in PDMS: **(d)** transmittance, **(e)** reflectance, and **(f)** absorptance. Dotted lines shown in panels d-f correspond to calculation results of a 6-μm-thick Si film.

was cured in a vacuum oven at 50°C for 3 hrs to fill the SiNW array. Then, flexible PDMS layers embedded with SiNW matrix were mechanically peeled from the Si wafers. The entire regions of the NWs were immersed inside PDMS, but the bottoms of them were exposed to air after peeling from the Si wafer. The optical reflectance and transmittance of NW embedded in PDMS were characterized using a UV–VIS/NIR spectrophotometer (Perkin-Elmer Lambda 750) equipped with an integrating sphere (60 mm) for collecting the diffused light. The optical transmittance, $T(\lambda)$, and reflectance, $R(\lambda)$, spectra of BS and AS were measured in the wavelength range from 400 to 1100 nm (Figure 1(d) and (e)) and compared with those of a 6-μm-thick film, which was obtained from calculations using the transfer matrix method (TMM). The optical absorptance, $A(\lambda) = 100 - T(\lambda) - R(\lambda)$, was estimated as shown in Figure 1(f). $A(\lambda)$ values of AS increased in the visible range ($500 < \lambda < 750$ nm) due to depression of $T(\lambda)$, which made the samples darker as clearly shown in the optical photographs (inset of Figure 1(c)). Also noteworthy is that the absorptance of AS in the NIR range ($\lambda \geq 750$ nm) is much larger than those of BS and 6-μm-thick film (Figure 1(f)). Since both $T(\lambda)$ and $R(\lambda)$ of AS decreased in the NIR range, the enhanced absorptance is resulting from the absorption by interaction of Au NPs and SiNWs. Regarding $A(\lambda)$ of AS, it should be clearly understood how large portion of light is absorbed in the SiNWs rather than being dissipated as Ohmic loss inside the NP. This is a critical concern for realizing high photoresponsivity of the plasmonic photodetectors [15-17].

The near-field interaction of the Au NPs with the SiNW was investigated using monochromated EELS, as shown in Figure 2. This technique could measure the LSP resonance energy in a single Au NP by subnanometer-sized e-beam at low energy range (<5 eV). The energy loss peaks lower than 1.3 eV (~950 nm) were not distinguishable because of a large full-width at half-maximum (FWHM: 0.25 – 0.35 eV) of the zero loss peak from the e-beam. The EELS spectra were obtained at four different positions ($P_1 - P_4$) in the TEM image of Figure 2(a), in which the P_1 and P_4 correspond to the cores of a hemispherical NP (hNP; 20 nm) and a spherical NP (sNP: 5 nm), respectively. P_2 and P_3 denote the hNP/SiNW interface and a SiNW, respectively. Except for P_3, all other positions show SP-related energy loss peaks: some portion of the incident electron energy is transferred to the LSP energy. For 20 nm-sized hNP, the single peak feature is observed at 2.4 eV (~520 nm) for P_1 and at 1.6 eV (~800 nm) for P_2, respectively (Figure 2(b)). The redshifted LSP resonance peak is observed at P_2 due to interaction between the oscillating free electrons in the hNPs and the charge carriers in the underlying Si [18,19]. Knight *et al.* found that the substrate with a larger permittivity would also give rise to a larger image charge with stronger interactions [19]. P_4 at the small NP, which has a spherical shape (as shown in Figure 2 (a)), has two peaks. The stronger peak at 3.0 eV and the weaker one at 2.5 eV are originated from the interband absorption and the LSP resonance, respectively. The interband transition in small-sized NPs (<10 nm) can have clear, intense feature contrary to the 20 nm-sized hNP, since electrons emerge as discrete energy levels in the NPs by their quantum size effect [23]. The LSP-related energy loss peak can be weakened for such small NPs because their dimensions are appreciably smaller (<10 nm) than a mean free path of oscillating electrons. The absorption feature at wavelengths below 600 nm reflects energy dissipation in NPs [23], not promoting absorption in the SiNWs. Thus, the broadband absorption enhancement in AS at NIR range ($\lambda > 750$ nm, Figure 1(f)) is mainly attributed to the LSP resonance at the hNP (>10 nm)/SiNW interfaces.

3-2 Simulation results

To understand the importance of the Au NP shape in the near-field interaction with the SiNW, spherical and hemispherical nanoparticle (sNP and hNP) with the same diameter of 20 nm were compared on semi-infinite

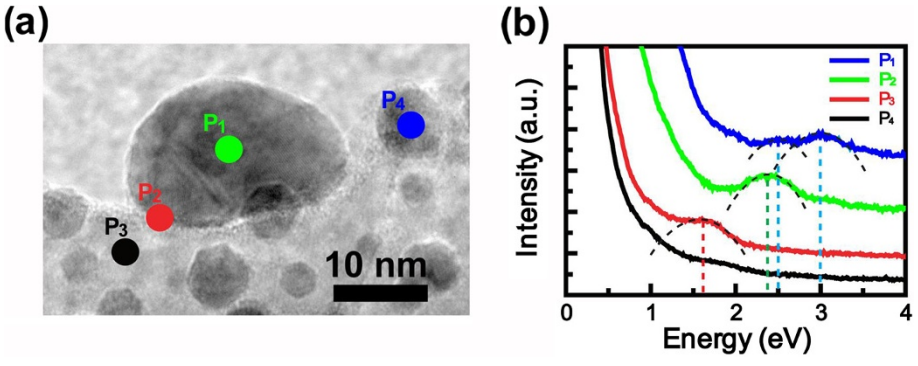

Figure 2 TEM and EELS characteristics of a Au NP-coated-SiNW. (a) TEM image of a Au NP-coated-SiNW. **(b)** EELS spectra extracted from the green (P_1), red (P_2), black (P_3), and blue (P_4) region in **(a)**.

Si substrate, as shown in Figure 3. Three dimensional (3D) simulations of an electromagnetic (EM) field were conducted using COMSOL multiphysics (ver. 4.2) based on a finite element method (FEM).

The total power absorbed by the single Au NP, $P_{abs,Au}(\omega)$, was calculated by integration of photon flux over a closed surface surrounding the NP;

$$P_{abs,Au}(\omega) = \int \frac{1}{2}\omega|E(\omega, x, y, z)|^2 \varepsilon_{Au}(\omega) dV \qquad (1)$$

in which ω, ε_{Au}, and $|E(\omega)|$ are the frequency of the light, the imaginary part of the Au permittivity, and the magnitude of the electric field, respectively. The absorption efficiency (Q_{abs}) of a single Au NP is defined as $Q_{abs}(\omega) = P_{abs,Au}(\omega)/[I_{in}(\omega)A_{geom}]$, where $I_{in}(\omega)$ and A_{geom} are the incident light intensity and the geometrical cross section, respectively. The Au sNP shows a single LSP resonance peak in the visible range: $\lambda = 500$ nm in air and 510 nm on Si (Figure 3(a)). The sNP contributes only slightly to the light absorption into a substrate even at the LSP resonance ($\lambda = \sim 500$ nm) because the strong LSP-induced near-field occurs far from the Si surface as shown in Figure 3(b). The hNP in air also shows a single peak at $\lambda = 520$ nm (Figure 3(c)). In contrast, the hNP on Si reveals two peaks at $\lambda = \sim 750$ nm and ~920 nm. At these wavelengths, substantial enhancement in a local field is observed at the hNP/Si interfaces (Figure 3(e)). As a comparison, similar field enhancement cannot be observed in the sNP/Si interface, as shown in Figure 3(d) ($\lambda = 920$ nm). All these results suggest that the NIR absorption peaks ($\lambda \geq 750$ nm) in AS should be caused by LSP-mediated field enhancement at hNP/SiNW interfaces. The slight variations in the peak positions between the experiments (Figure 2(b)) and the simulations (Figure 3(a)) can be originated from the consideration of a specific size of the hNP (i.e., 20 nm) and a simplified Si geometry (i.e., planar wafer) given in the simulation.

Figure 4(a) shows the absorption enhancement spectra of AS arrays with different NP size (diameter: 20, 30, and 40 nm), obtained by the FEM simulations. The selected NP sizes cover the statistical distribution of the NPs (Figure 1(c)). Small-sized NPs (<10 nm) were disregarded since their contribution to the absorption in SiNW is negligible as aforementioned. The unit cells, representing periodic BS and AS arrays, were modelled in the simulation. Monochromatic plane waves with polarization parallel to the x-axis were incident from the top of the NW array along the z axis. Boundary conditions of perfect magnetic conductors (PMCs) were used for $y = 0$ and $y = p/2$ planes (p: period of the NW array), and perfect electric conductor (PEC) conditions were used for the other two planes, $x = 0$ and $x = p/2$. Perfect matched layer (PML) boundary conditions were used at the top and bottom faces of the unit cell. As a result, the electric field could be mirrored to the whole periodic space. Geometric parameters of the NW arrays were chosen to have the representative values of SiNW arrays used in the experimental studies: diameter (d) = 60 nm, $p = 100$ nm, and a space filling ratio (FR = $\pi d^2/4p^2 = 0.28$). A length of NW was fixed 1 μm because the most of NPs were found within 1 μm from the top-ends of the SiNW array. For the sake of simplicity, an ordered arrangement of the Au hNPs was assumed in the calculations: four hNPs were orthogonally placed around a SiNW at the same height and nine pairs of the hNP were positioned along the axial direction of 1-μm-long SiNWs with a pitch of 100 nm.

The theoretical absorption enhancement in SiNW is defined as the absorbed power of SiNW in AS divided by that of BS. The absorbed power in the SiNW ($P_{abs,SiNW}$) can be evaluated through the integration of the photon

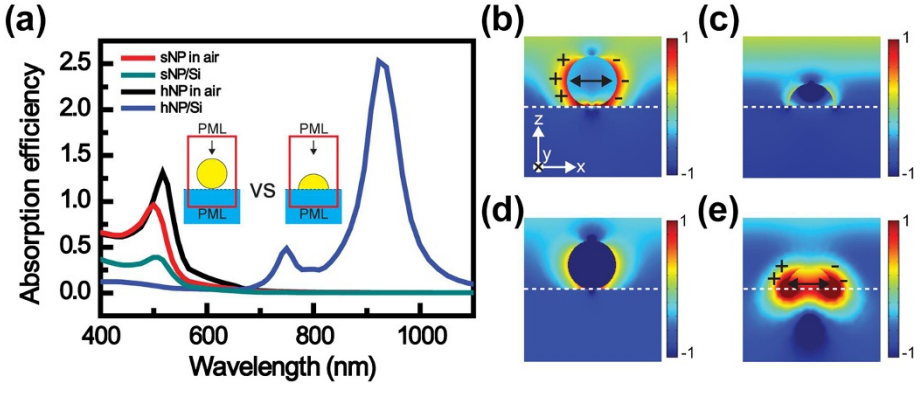

Figure 3 Absorption efficiency and electric field intensity for single Au sNP and hNP. (a) Absorption efficiency spectra of single Au sNP and hNP (20 nm) in air and on a planar Si substrate, respectively. A perfectly-matched-layer (PML) boundary condition was used for the simulation volume surface. Incident light is a plane wave propagating along the –z axis and linearly polarized along the x axis. Cross-sectional distributions of the electric-field intensity at a NP/Si interface are shown for wavelengths of **(b, c)** 500 nm and **(d, e)** 920 nm.

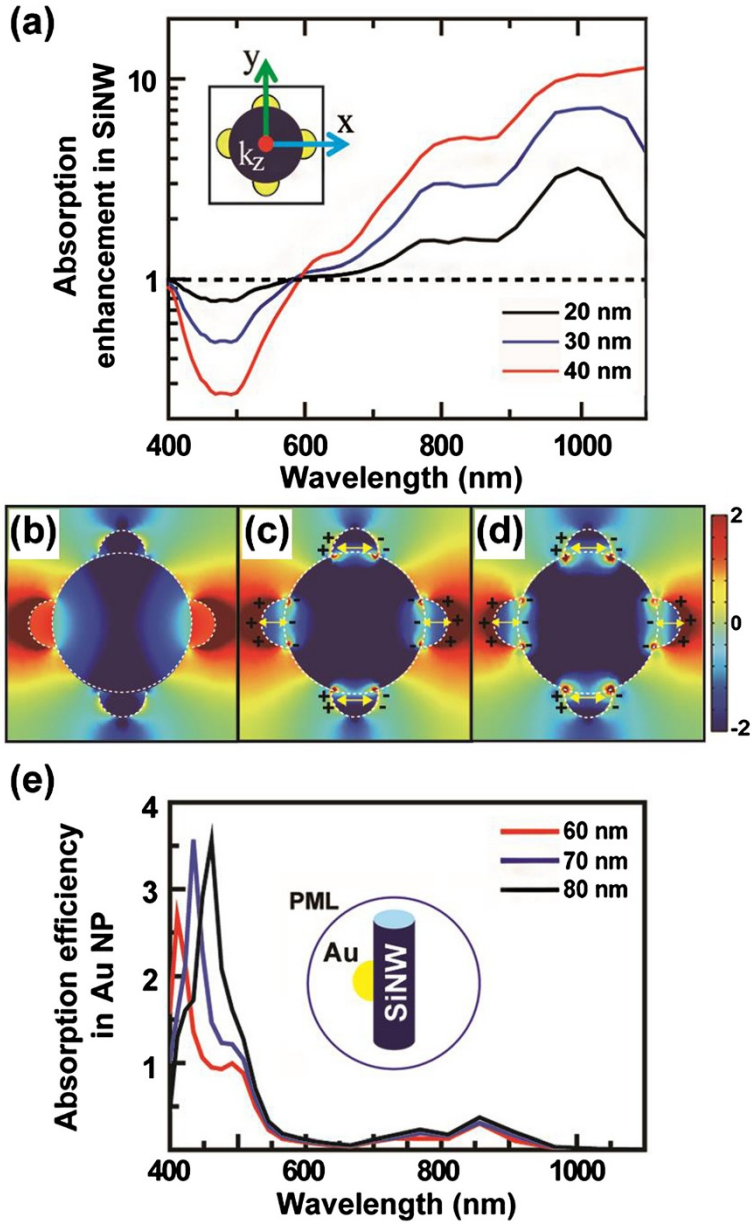

Figure 4 Absorption enhancement spectra for SiNW array coated with NPs. (a) Absorption enhancement spectra (simulation) of the SiNW arrays coated with NPs (20 nm for black, 30 nm for blue, and 40 nm for red). Inset shows a cross-sectional top-view of a unit cell for simulation in the x-y plane. k_z represents a wave vector of the incident light and the electric-field is polarized along the x axis. **(b-d)** Distributions of the electric-field intensity in a unit cell of the array are shown for wavelengths of 490, 800, and 1000 nm in the x-y plane, respectively. Yellow arrows inside Au hNPs represent dipolar oscillations. **(e)** Absorption efficiency (Q_{abs}) spectra of Au NP for a single Au NP-coated SiNW (A spherical PML: blue circle in inset).

flux within the volume of the SiNW according to a following equation,

$$P_{\mathrm{abs,SiNW}}(\omega) = \int_{\mathrm{SiNW}} \frac{1}{2}\omega |E(\omega, x, y, z)|^2 \varepsilon_{\mathrm{Si}}(\omega) dV \qquad (2)$$

in which $\varepsilon_{\mathrm{Si}}(\omega)$ is the imaginary part of the Si permittivity. The absorption enhancement exhibits two broad peaks at ~800 and ~1000 nm, corresponding to the LSP resonance wavelengths. Upon increasing the NP size from 20 nm to 40 nm, the enhancement at $\lambda = 1000$ nm is also increased from 2 to 10 due to the stronger LSP – substrate interaction. Local hot spots along the perimeters of the hNP/SiNW interface are observed in the simulated field distribution (Figure 4(c) and (d)) so that each hNP, as an optical NA, concentrates the incoming light into a strongly localized field. Very interestingly, field enhancement is observed not only around the NPs placed along

the polarization direction (x axis), but also those placed orthogonally (y axis) to the polarization direction. This clearly demonstrates a beneficial role of the NW geometry for enhanced near-field coupling that minimizes the directional limitation of light polarization. In addition, we could also understand the reason why the simulation results assuming the periodic arrangement of NPs show good agreement with the experimental data obtained from randomly coated NPs on SiNWs. The NP-induced field enhancement is as large as 63 at the wavelength of ~1000 nm. The NIR absorption is enhanced with increasing NP size and the peak is further red-shifted due to the enlarged contact area of the NP/SiNW (Figure 4(a)).

The absorption of the NP-coated SiNWs is smaller than that of the bare SiNWs at $\lambda < 600$ nm (Figure 4(a)); it has a minimum of $\lambda = 490$ nm, corresponding to the guided mode resonance of SiNW ($d = 60$ nm). The SiNWs show strong absorption at their resonance modes. The resonant wavelength is determined by the NW diameter, d: for example, $\lambda = 550$–750 nm for $d = 90$–140 nm [4]. At $\lambda = 490$ nm (Figure 4(b)), a large electric field is seen inside the bulk of hNPs, indicating significant absorption by the Au hNP. Strong radiation from the hNPs is also observed along the polarization direction of the incident light (x axis). These features show that much of incoming light is absorbed in the Au NPs and reradiated into air rather than absorbed in the SiNWs. In order to examine the influence of the guided mode resonance, the $Q_{abs,\ Au}$ for a single Au NP attached on a SiNW, with $d = 60$, 70, and 80 nm, was compared. A spherical perfectly matched layer (PML: blue circle in inset) with a thickness of 30 nm and a radius of 200 nm was introduced to absorb the light scattered by the Au NP and SiNW. As shown in Figure 4(e), the $Q_{abs}(\omega)$ of the Au hNP (diameter: 20 nm) has two peaks; a larger one at $\lambda < 600$ nm and a smaller one at $\lambda > 800$ nm are related to the NW-guided-mode resonance and LSP-mediated resonance, respectively. The peak position for the former is well matched with the guided mode resonance wavelengths, as reported [4]. The peaks for the latter are nearly invariant because the NP size is fixed. Note that the Au hNPs perturb the optical confinement of the resonance modes in the SiNWs; moreover, suppress visible range ($\lambda < 600$ nm) optical absorption enhancement in the SiNWs as shown in Figure 4(a).

3-3 Electrical characteristics

Spectral responsivities for the BS and AS devices are measured, as shown in Figure 5a. A schematic diagram of our device is illustrated in the inset of Figure 5(a). The responsivity (R) can be given by the following equation;

$$R = \frac{I_{light} - I_{dark}}{P_{inc}} \tag{3}$$

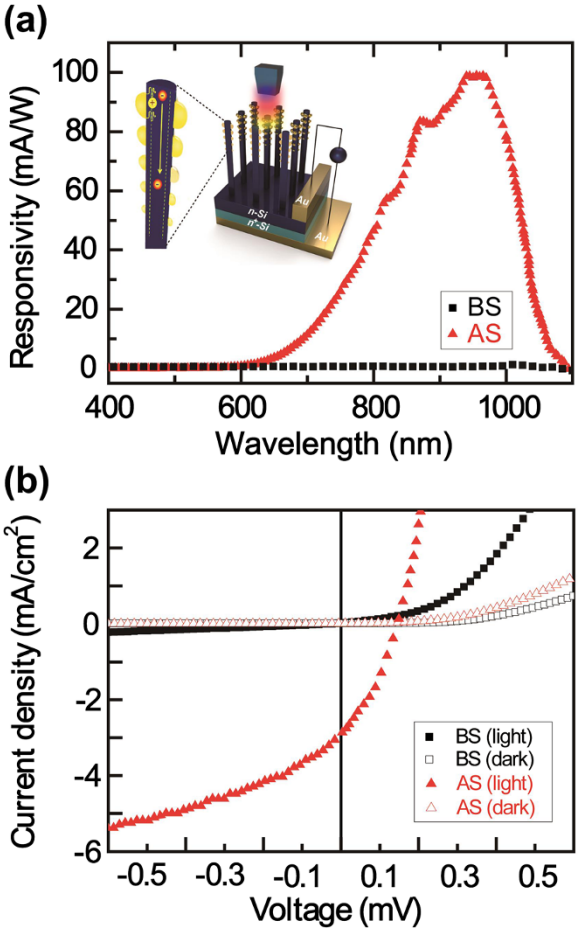

Figure 5 Responsivity spectra and J-V plots for SiNWs with and without Au NPs. (a) Responsivity (experimental) spectra for BS (black), AS (red) photodetectors. (Inset is schematic illustration of our photodetector consisting of Au hNP-coated SiNWs.) **(b)** The *J-V* curves of the SiNW photodetectors without (BS for black) and with Au NPs (AS for red). Open and filled symbols indicate *J-V* curves in dark and under illumination at AM 1.5G, respectively.

where I_{light}, I_{dark}, and P_{inc} are the current under illumination, the dark current, and the incident illumination power, respectively. R of the BS device is nearly zero over the entire wavelength range, whereas R of the AS device is very large at wide wavelength range. R approaches zero as the photon energy becomes smaller than the bandgap of Si (i.e., $\lambda = \sim 1{,}100$ nm). R of the AS device has a broad peak in the NIR region, where the absorption enhancement appears from the experiments (Figure 1(f)) and simulation (Figure 4(a)).

Figure 5(b) shows the current density-voltage (*J-V*) characteristics of the BS and AS devices under dark and light illumination at AM 1.5G. The *J-V* curves under both conditions exhibit a rectifying behavior since the Au top-electrodes (finger bar) form Schottky contacts with n-Si substrate. The short circuit current density (J_{sc}) and the open circuit voltages (V_{oc}) for the BS device

are only 0.2 mA/cm^2 and nearly zero, respectively. J_{sc} and V_{oc} of the AS device are estimated to be 2.9 mA/cm^2 and 150 mV, respectively. In the BS device, the photogenerated electron–hole pairs (EHPs) suffer from severe recombination in Si before reaching the electrodes. On the other hand, the Au NPs can also act as a Schottky junctions in contact to a SiNW surface for spatially separating the photogenerated EHPs into the orthogonal direction to the NW axis, driven by the built-in-field in space charge region (SCR) (inset in Figure 5(a)). As the excited electrons reach a neutral region of *n*-type Si bulk, a charge state of a substrate tends to be more negative, which results in further enhancement of *n*-type conductance. This explains why the larger J_{sc} and V_{oc} were observed from the NPs-coated SiNW devices compared to those of BS.

4 Conclusions

We have demonstrated that the vertical SiNW array coated with Au hemispherical nanoparticles (hNPs) exhibit remarkable performance as a near-infrared (NIR) photodetector, compared with the bare SiNW array. Experimental and simulation results clearly show that the Au hNPs (>10 nm) act as nanoantennas, then induce strong NIR absorption. hNPs suppress the guided-mode-induced absorption in SiNW for reducing a visible range photocurrent. This allows the hNP-coated SiNW array to possess the unique NIR-selective response. The Schottky contact formation at the hNP/SiNW interface supports the photo-excited carrier separation and improves the responsivity. Our devices offer an alternative route for conventional NIR photodetectors based on a microfabrication method, without the need of any cost-increasing procedures.

Competing interests

The authors declare that they have no competing interest.

Authors' contributions

SWJ carried out experimental work. SWJ, JHL, and DWK analysed the data to draw physical insights. KZ carried out the calculations and plotted simulation results. SWJ, KZ, DWK, JHL wrote the article and approved the final manuscript. All authors read and approved the final manuscript.

Acknowledgements

This work was supported by the National Research Foundation of Korea (NRF) grant funded by the Korea government (MSIP) (No. 2011–0028604). This work was also supported by the Human Resources Development program **(No. 20124030200130)** of the Korea Institute of Energy Technology Evaluation and Planning (KETEP) grant funded by the Korea government Ministry of Trade, Industry and Energy.

Author details

[1]Department of Chemical Engineering, Hanyang University, Ansan 426-791, South Korea. [2]Department of Physics, Ewha Womans University, Seoul 120-750, South Korea. [3]Department of Mechanical Engineering, Texas A&M University, College Station, TX, USA. [4]Department of Physics, Harbin Institute of Technology, Harbin, China.

Received: 4 September 2014 Accepted: 14 September 2014
Published online: 12 November 2014

References

1. M Csutak, JD Schaub, WE Wu, JC Campbell IEEE Photon. Tech. Lett. **14**, 516 (2002)
2. J Michel, J Liu, LC Kimerling, Nat. Photon. **4**, 527 (2010)
3. AM Joshi, FJ Effenberger, M Grieco, G Feng, W Zhong, J Ott. Proc. SPIE **2290**, 430 (1994)
4. K Seo, M Wober, P Steinvurzel, E Schonbrun, Y Dan, T Ellenbogen, K Crozier Nano Lett. **11**, 1851 (2011)
5. T Kempa, J Cahoon, S-K Kim, R Day, D Bell, H-G Park, C Lieber. Proc. Natl. Acad. Sci. U. S. A. **109**, 1407 (2012)
6. BC Sturmberg, KB Dossou, LC Botten, AA Asatryan, CG Poulton, CM De Sterke, RC McPhedran. Opt. Express **19**, A1067 (2011)
7. J Zhu, Z Yu, G Burkhard, C-M Hsu, S Connor, Y Xu, Q Wang, M McGehee, S Fan, Y Cui. Nano Lett. **9**, 279 (2009)
8. J-Y Jung, Z Guo, S-W Jee, H-D Um, K-T Park, J-H Lee. Opt. Express **18**, A286 (2010)
9. L Hu, G Chen. Nano Lett. **7**, 3249 (2007)
10. Q Du, C Kam, H Demir, H Yu, X Sun. Opt. Lett. **36**, 1884 (2011)
11. M Kelzenberg, S Boettcher, J Petykiewicz, D Turner-Evans, M Putnam, E Warren, J Spurgeon, R Briggs, N Lewis, H Atwater. Nat. Mater. **9**, 239 (2010)
12. KQ Peng, ST Lee. Adv. Mater. **23**, 198 (2011)
13. B Tian, X Zheng, TJ Kempa, Y Fang, N Yu, G Yu, J Huang, CM Lieber. Nature **449**, 885 (2007)
14. K Zhou, S-W Jee, Z Guo, S Liu, J-H Lee. Appl. Opt. **50**, G63 (2011)
15. S Brittman, H Gao, EC Garnett, P Yang. Nano Lett. **11**, 5189 (2011)
16. JK Hyun, LJ Lauhon. Nano Lett. **11**, 2731 (2011)
17. VE Ferry, JN Munday, HA Atwater. Adv. Mater. **22**, 4794 (2010)
18. KR Catchpole, A Polman. Appl. Phys. Lett. **93**, 191113 (2008)
19. MW Knight, Y Wu, JB Lassiter, P Nordlander, NJ Halas. Nano Lett. **9**, 2188 (2009)
20. KB Crozier, A Sundaramurthy, GS Kino, CF Quate. J. Appl. Phys. **94**, 4632 (2003)
21. V Giannini, AI Fernandez-Dominguez, SC Heck, SA Maier. Chem. Rev. **111**, 3888 (2011)
22. MW Knight, H Sobhani, P Nordlander, NJ Halas. Science **332**, 702 (2011)
23. B Balamurugana, T Maruyama. Appl. Phys. Lett. **87**(143), 105 (2005)

doi:10.1186/s40580-014-0029-z
Cite this article as: Jee *et al.*: A silicon nanowire photodetector using Au plasmonic nanoantennas. *Nano Convergence* 2014 **1**:29.